Effects of chemical and hydrostatic pressures on structural, magnetic, and electronic properties of R_2NiMnO_6 (R = rare-earth ion) double perovskites

Hong Jian Zhao,[1,2] Xiao Qiang Liu,[1] Xiang Ming Chen,[1,*] and L. Bellaiche[2,†]

[1]*Laboratory of Dielectric Materials, Department of Materials Science and Engineering, Zhejiang University, Hangzhou 310027, China*

[2]*Institute for Nanoscience and Engineering and Physics Department, University of Arkansas, Fayetteville, Arkansas 72701, USA*

(Received 26 July 2014; revised manuscript received 22 September 2014; published 25 November 2014)

The effects of chemical and hydrostatic pressures on structural, magnetic, and electronic properties of R_2NiMnO_6 double perovskites, with R being a rare-earth ion, have been systematically studied by using specific first-principles calculations. These latter reproduce well the correlation between several properties (e.g., lattice parameters, Ni-O-Mn bond angles, magnetic Curie temperature, and electronic band gap) and the rare-earth ionic radius (i.e., the chemical pressure). They also provide novel predictions awaiting experimental confirmation, such as (i) that many physical quantities respond in dramatically different manners to chemical versus hydrostatic pressure, unlike as commonly thought for perovskites containing rare-earth ions, and (ii) a dependence of antipolar displacements on chemical and hydrostatic pressures, which would further explain why the recently predicted electrical polarization of La_2NiMnO_6/R_2NiMnO_6 superlattices [H. J. Zhao, W. Ren, Y. Yang, J. Íñiguez, X. M. Chen, and L. Bellaiche, Nat. Commun. **5**, 4021 (2014)] can be created and controlled by playing with the rare-earth element.

DOI: 10.1103/PhysRevB.90.195147 PACS number(s): 75.30.Kz, 61.50.−f

I. INTRODUCTION

Perovskites made of R_2NiMnO_6 (with R being a rare-earth ion) are ferromagnetic semiconductors that have attracted increasing scientific attention [1–4], partly because their magnetic Curie temperature is rather high and can be tuned by varying the rare-earth element. From a structural point of view, these systems adopt two different space groups for their ground state, depending on the atomic arrangement between the Ni and Mn atoms. More precisely, a random distribution of B (with B = Ni or Mn) ions results in an orthorhombic *Pbnm* symmetry. On the other hand, a rock-salt ordering (for which all first nearest neighbors of Ni atoms in the B sublattice are Mn atoms and vice versa) leads to a monoclinic $P2_1/n$ symmetry [1–3], with the resulting compounds usually being termed R_2NiMnO_6 *double perovskites*. Furthermore, and in contrast with the double perovskite La_2NiMnO_6 (which is a *room temperature* ferromagnetic semiconductor) [5–8], properties of R_2NiMnO_6 double perovskites possessing $4f$ electrons have been much less investigated [1–4]—especially at a theoretical/computational level. One may thus wonder if specific first-principles calculations can overcome the difficulty in mimicking well the localized d electrons of both Ni and Mn ions and their effect on physical quantities of R_2NiMnO_6 double perovskites. In other words, it will be useful to determine, for example, what precise functional in density functional theory can reproduce some known features of these materials, such as the systematic decrease [2] of the Ni-O-Mn bond angles and of the magnetic Curie temperature (T_C) by decreasing the rare-earth ionic radius, r_R [9], and the increase of electronic band gaps of R_2NiMnO_6 double perovskites when R changes from La to Sm [1]. Such determination will also allow scientists to trust the predictions of these first-principles calculations for other important properties of R_2NiMnO_6 double perovskites that have not been experimentally reported, to the best of our knowledge. Examples include (i) the magnitude of the *antipolar* displacements of the R_2NiMnO_6 double perovskites, which is a highly desired piece of information to have, taking into consideration that the difference in magnitude of these antipolar displacements between different rare-earth elements has been recently proposed [10–12] to be responsible for the formation and control of the electrical polarization of La_2NiMnO_6/R_2NiMnO_6 superlattices (and which thus renders such systems *multiferroic near room temperature* according to Ref. [13]); and (ii) the effect of *hydrostatic* pressure on structural, magnetic, and electronic properties of R_2NiMnO_6 double perovskites. In particular, it will be useful to determine if hydrostatic and chemical pressures have the same effect on properties of rare-earth-based materials, as advocated in Ref. [14].

The aim of this paper is to address all the aforementioned unresolved issues by performing and analyzing specific first-principles calculations on R_2NiMnO_6 double perovskites.

II. COMPUTATIONAL DETAILS

In the present paper, we focus on the properties of the B-site-ordered double perovskite R_2NiMnO_6 (thus having the $P2_1/n$ symmetry). We also adopt a ferromagnetic ordering since such double perovskites are classical oxides verifying the Goodenough-Kanamori rule; i.e., the Ni e_g^2-Mn e_g^0 superexchange interaction leads to ferromagnetic ordering of Ni and Mn spin vectors [2]. The first-principles calculations are performed by the Vienna *Ab initio* Simulation Package (VASP) code [15] with the exchange correlation functional being described in the framework of Perdew-Burke-Ernzerhof revised for solids (PBEsol) [16] within the generalized gradient approximation (GGA). The Monkhorst-Pack k-point mesh of (6, 6, 4) is chosen for Brillouin-zone integration. The projector-augmented wave (PAW) method

*xmchen59@zju.edu.cn

†laurent@uark.edu

is used for the following valence electronic configurations: $5s^2 5p^6 5d^1 6s^2$ for Ce, Pr, Nd, and Sm; $5p^6 5d^1 6s^2$ for Gd, Tb, Dy, Ho, and Er; $3d^9 4s^1$ for Ni; $3d^6 4s^1$ for Mn; and $2s^2 2p^4$ for O. The $4f$ electrons of rare-earth elements are treated as core states in the present calculations since (i) partially filled $4f$ states typically lead to convergence problems [15], and (ii) freezing $4f$ electrons in the core has a very weak effect on structural and high-temperature magnetic properties of perovskite compounds possessing rare-earth ions at their A sites, as demonstrated in Refs. [13,17,18]. The energy cutoff is selected as 500 eV. The structural optimization is performed with the atomic force convergence criteria of 0.005 eV/Å. The GGA plus Hubbard U method is implemented in the present calculations, choosing the effective Hubbard U parameters of 3.0 eV for both Ni^{2+} and Mn^{4+}. As we will see, such Hubbard U values reproduce rather well the experimental magnetic Curie temperature of rock-salt-ordered R_2NiMnO_6 systems, once the numerical values are rescaled by a factor of 0.430. Note that these numerical values for the magnetic Curie temperature of R_2NiMnO_6 are obtained via the mean field approximation (MFA) giving $T_C = (E_{FiM} - E_{FM})/6k_B$, where E_{FiM} and E_{FM} are the energy of ferrimagnetic and ferromagnetic states per formula unit, respectively, and k_B is the Boltzmann constant (the spin vectors of Ni^{2+} and Mn^{4+} sublattices are parallel to each other in the ferromagnetic state, whereas they are antiparallel to each other in the ferrimagnetic state). Note that this way of determining T_C implies that only the first nearest neighbor exchange interactions between Ni and Mn atoms are assumed to contribute to magnetism, which is justified for the chemically ordered double perovskite in this paper (although it will be invalid for disordered systems for which first nearest neighbor Ni-Ni and Mn-Mn interactions will exist and thus will also play a role on magnetism). Note also that we performed additional calculations, for which the Hubbard U values of both Ni and Mn have been varied within PBEsol, as well as use the PBE functional [19] with $U = 3$ eV for both Ni and Mn in order to determine the influence of the Hubbard correction and functional on properties of R_2NiMnO_6 double perovskites.

III. RESULTS AND DISCUSSION

First, we focus on the effects of chemical pressure (i.e., the rare-earth ionic radius r_R [9]) on structural properties of R_2NiMnO_6 double perovskites (see Fig. 1). The lattice parameters, as well as monoclinic angles, reported in Fig. 1(a) show three main characteristics: (i) for R = Nd to Er, the lattice parameter b is the largest and a is the smallest (for R = Ce, however, a is the largest while b and $c/\sqrt{2}$ are very close to each other; for R = Pr, a, b, and $c/\sqrt{2}$ are all close to each other); (ii) a and $c/\sqrt{2}$ decrease (almost linearly) with decreasing r_R, while b first increases with decreasing r_R and then stays more or less constant for R = Gd, Tb, Dy, Ho, and Er; and (iii) the monoclinic angle β meanwhile increases from ~89.9° to 90.7°. Items (i)–(iii) are all consistent with experiments [2], and the calculated lattice parameters a, b, and c are slightly underestimated by less than 1.5%, 0.6%, and 1.1%, respectively, from measurements [2]. Such facts therefore attest to the accuracy of the simulations. Moreover, Fig. 1(b) shows that the mean Ni-O bond length first increases when R changes from Ce to Gd, then remains nearly unchanged for R = Gd, Tb, Dy, Ho, and Er, similar to the

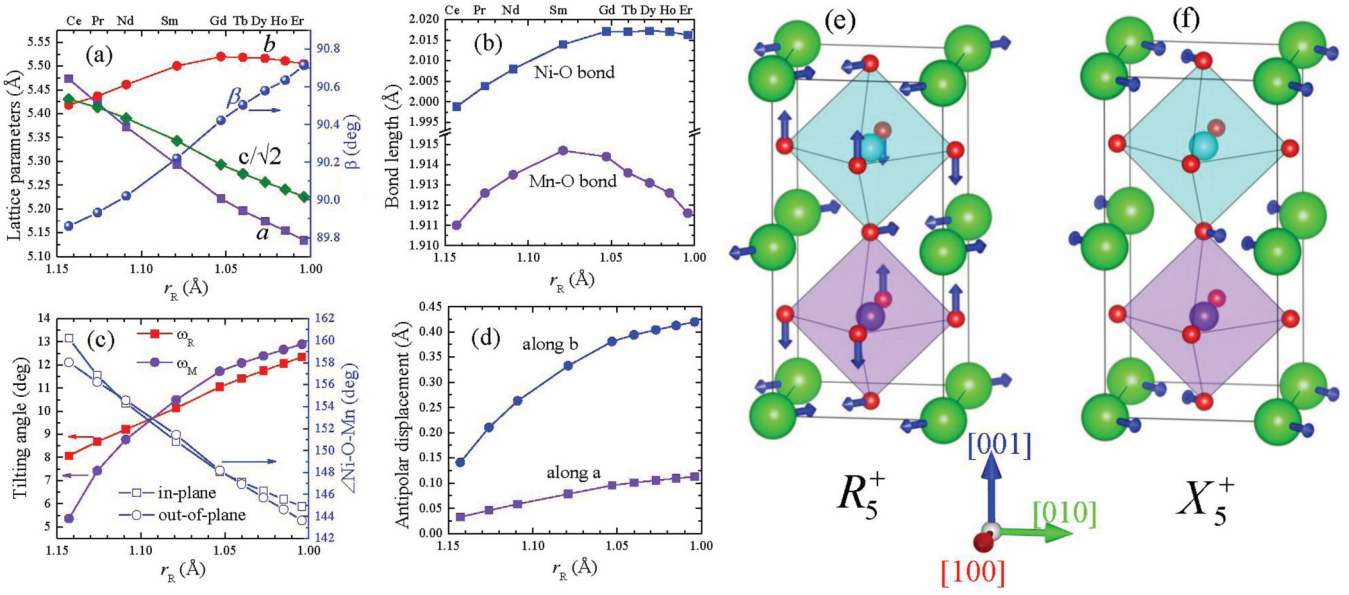

FIG. 1. (Color online) Structural properties of R_2NiMnO_6 double perovskite oxides as a function of chemical pressure (i.e., the rare-earth ionic radius, r_R). (a) Lattice parameters a, b, c and monoclinic angle β; (b) Ni-O and Mn-O bond lengths; (c) the average antiphase tilting ω_R (about the pseudocubic [100] or [010] direction), in-phase tilting ω_M (about the pseudocubic [001] direction), and in-plane and out-of-plane Ni-O-Mn bond angles; (d) antipolar displacement of the R ions. Panels (e) and (f) schematize the patterns associated with the antipolar displacements discussed in the text, with the pseudocubic [100], [010], and [001] directions also indicated there. The light blue and purple colors are used to represent NiO_6 and MnO_6 octahedrons, respectively. The AFE displacements associated with the R point (e) and X point (f) of the cubic first Brillouin zone are along the pseudocubic [1$\bar{1}$0] direction (which is the a axis) and pseudocubic [110] direction (which is the b axis), respectively.

behavior of the b lattice constant. On the other hand, the mean Mn-O bond length first increases then decreases (showing a maximum value for Sm_2NiMnO_6) when R changes from Ce to Er. Such nonmonotonic behavior implies that one should, in fact, distinguish between two sets of rare-earth ions: one set ranging between Ce and Sm and another set ranging between Gd and Er. Interestingly, some recent papers also found that these two sets of rare-earth ions can adopt different behaviors in other systems. For instance, Ref. [17] showed that these two sets differ in the orthoferrites by (i) the average value of the rare-earth ion chemical charge; (ii) the hierarchy between the value of the magnetization of the Γ_2 spin configuration and that of the Γ_4 spin configuration; and (iii) the behavior of the b lattice parameter, of some bond lengths, and bond length splitting as a function of the rare-earth ionic radius. It is also interesting to notice that the mean Ni-O bond length shown in Fig. 1(b) is larger than the mean Mn-O bond length for any R_2NiMnO_6 double perovskite. Note that the calculated mean Ni-O and Mn-O bond lengths typically differ by less than 2.6% and 1.1%, respectively, compared with experiments [2].

According to Glazer's notation [20], the tilting pattern of R_2NiMnO_6 is $a^-a^-c^+$. In other words, there is a pseudovector, ω_R, characterizing the averaged antiphase tilting that lies about the pseudocubic [110] direction (which is the b axis), and there is another pseudovector, ω_M, representing the averaged in-phase tilting about the [001] pseudocubic direction (which is the c axis). Note that the magnitudes of ω_R and ω_M quantify the values of the tilting angles while their direction is the axis about which oxygen octahedral tilt [21,22]. Figure 1(c) shows that the x and y components of ω_R are increased from 8.1° to 12.3° while the z component of ω_M is enhanced from 5.3° to 12.9° when R changes from Ce to Er (the x, y and z axes are chosen here to lie along the pseudocubic [100], [010], and [001] directions, respectively). Such variations result in a decrease from 160.2° to 144.9° (respectively, from 158.0° to 143.6°) for the averaged in-plane (respectively, out-of-plane) Ni-O-Mn bond angle, as is consistent with experiments [2]. (Note that the plane we are referring to, when using the in-plane versus out-of-plane terminology, is the (001) plane, that is, the one perpendicular to the c or, equivalently, z axis). These predicted bond angles typically differ by 2.3% from measurements of Ref. [2], which further quantifies the accuracy of the calculations. Moreover, it is now known [23] that, for the $a^-a^-c^+$ tilting pattern, the combination of antiphase tilting ω_R and in-phase tilting ω_M leads (via specific coupling energy terms) to the occurrence of two different antiferroelectric (AFE) displacements of the A ions in perovskite compounds: As schematized in Figs. 1(e) and 1(f), one type (R_5^+) is associated with the R point of the cubic Brillouin zone, with an AFE vector being along the a axis and a second type (X_5^+) associated with the X point, for which the AFE vector lies along the b axis. The magnitude of the AFE displacements of the R^{3+} ion in the R_2NiMnO_6 double perovskites along the a and b directions of the $P2_1/n$ phase is shown in Fig. 1(d). When R changes from Ce to Er, the AFE displacements of R^{3+}ions along the a and b directions both increase. The magnitude of the AFE displacements along the b direction is always larger than that along the a direction. Note that the behavior of the AFE displacements shown in Fig. 1(d) as a function of the chemical pressure is offered here as a prediction to be experimentally checked. The difference in magnitude of these AFE motions between different R ions has been recently shown [13,18] to be responsible for the ferroelectric origin of R_2NiMnO_6/La_2NiMnO_6 superlattices (which thus are multiferroics near room temperature), according to Ref. [13].

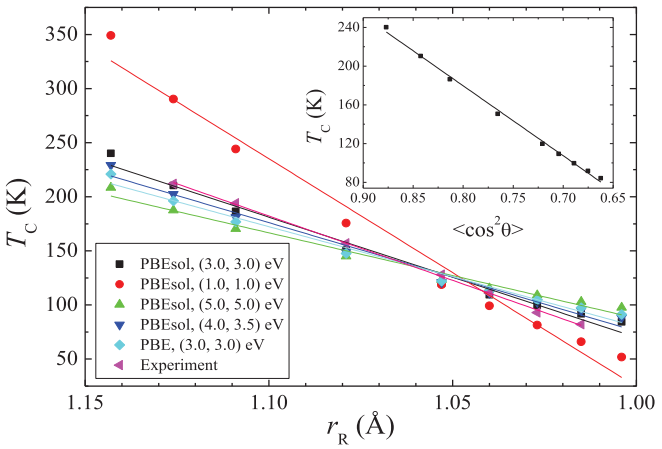

FIG. 2. (Color online) Magnetic Curie temperature, T_C, of R_2NiMnO_6 double perovskite oxides as a function of chemical pressure calculated via the PBEsol and PBE functionals for different effective Hubbard U values for Ni and Mn ions (U_{Ni}, U_{Mn}). The inset shows T_C as a function of the mean value of $\cos^2\theta$, with θ being the Ni-O-Mn bond angle, for the PBEsol functional with ($U_{Ni} = 3$ eV, $U_{Mn} = 3$ eV).

We now investigate the magnetic properties of R_2NiMnO_6 double perovskites. Figure 2 shows the magnetic Curie temperature as a function of chemical pressure. One first notices that the calculated Curie temperatures agree very well with the experimental values [2]. Such agreement explains why we selected a Hubbard U parameter of 3.0 eV for both Ni^{2+} and Mn^{4+} ions, as well as decided to adopt the aforementioned rescaling of the numerical magnetic Curie temperatures. Second, one can also see that the correlation between the Curie temperature and rare-earth ionic radius is monotonic, with the Curie temperature decreasing as r_R decreases. To understand such dependency, the inset of Fig. 2 reports the Curie temperature of R_2NiMnO_6 double perovskites as a function of their mean value of $\cos^2\theta$, where θ is the Ni-O-Mn bond angle, which is often termed the superexchange angle [24]. (Practically, $\langle\cos^2\theta\rangle$ in the inset of Fig. 2 is calculated as two-thirds the square of the in-plane Ni-O-Mn bond angle added to one-third the square of the out-of-plane Ni-O-Mn bond angle.) This inset reveals a "perfect" linear (increasing) relationship between the Curie temperature and $\langle\cos^2\theta\rangle$, in agreement with the experimental data in Ref. [2], and indicates that chemical pressure affects the Curie temperature mostly by changing the tilting angles [consistent with Fig. 1(c) showing that smaller r_R gives larger ω_R and ω_M].

Figure 2 also reports the predicted Curie temperature when using different Hubbard U values between Ni and Mn, as well as the same U corrections for Ni and Mn but with a value different from 3 eV within the PBEsol functional. Figure 2 reveals that the selection of $U = 3$ eV for both Ni and Mn provides the best agreement with experiments once rescaling

is done, which further explains our present choice (note that the rescaling factor was numerically found to be equal to 0.681, 0.428, and 0.338 when ($U_{Ni} = 1.0$ eV, $U_{Mn} = 1.0$ eV), ($U_{Ni} = 4.0$ eV, $U_{Mn} = 3.5$ eV), and ($U_{Ni} = 5.0$ eV, $U_{Mn} = 5.0$ eV), respectively. Moreover, Fig. 2 also indicates that the PBE and PBEsol functionals, both using $U = 3$ eV for Ni and Mn, give similar results for the behavior of T_C with the rare-earth ionic radius, albeit PBEsol yields predictions that agree slightly better with measurements. Note that the rescaling factor was found to be 0.505 for the PBE functional with ($U_{Ni} = 3.0$ eV, $U_{Mn} = 3.0$ eV).

Let us now reveal the effect of hydrostatic pressure on properties of a specific R_2NiMnO_6 double perovskite, namely Sm_2NiMnO_6. The idea here is to check if applying hydrostatic pressure on Sm_2NiMnO_6 has the same effect as the chemical pressure in R_2NiMnO_6 on structural and magnetic quantities, as was recently advocated for rare-earth-doped $BiFeO_3$ [14] but not for rare-earth orthoferrites and orthochromates [17,18]. For that, we first determine the precise value of the hydrostatic pressures needed for the cell volume of Sm_2NiMnO_6 to be equal to that of the ground state (i.e., without hydrostatic pressure) of R_2NiMnO_6 oxides (with R = Ce to Er). Such critical hydrostatic pressures are found to be around −60, −45, −30, 0, 38, 56, 73, 90, and 107 kbar, corresponding to Ce, Pr, Nd, Sm, Gd, Tb, Dy, Ho, and Er, respectively. Figures 3 and 4 compared with Figs. 1 and 2 show that, in fact, chemical and hydrostatic pressures affect several properties of R_2NiMnO_6 double perovskites in a rather different way. For instance, the lattice parameters a, b, and c, as well as the averaged Ni-O and Mn-O bond lengths of Sm_2NiMnO_6,

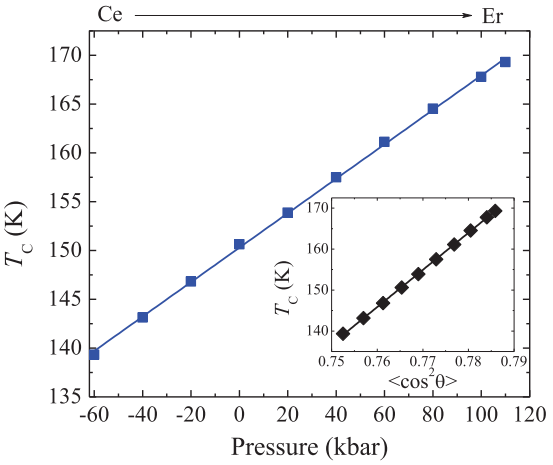

FIG. 4. (Color online) Similar to Fig. 2, but for Sm_2NiMnO_6 double perovskite as a function of hydrostatic pressure.

all monotonically decrease (in an almost linear fashion) with increasing hydrostatic pressure, and the monoclinic angle is nearly unchanged by a hydrostatic pressure. In addition, the relationship $b > c/\sqrt{2} > a$ remains valid in the entire investigated hydrostatic pressure range, which, once again, contrasts with the behavior of lattice parameters with chemical pressure. Another main difference between these two different pressures is that the ω_R and ω_M tilting angles both decrease (from 10.5° to 9.6° for ω_R, and from 10.6° to 10.1° for ω_M), which results in an increase of the mean Ni-O-Mn bond angles (from 150.2° to 152.0° for the in-plane angle

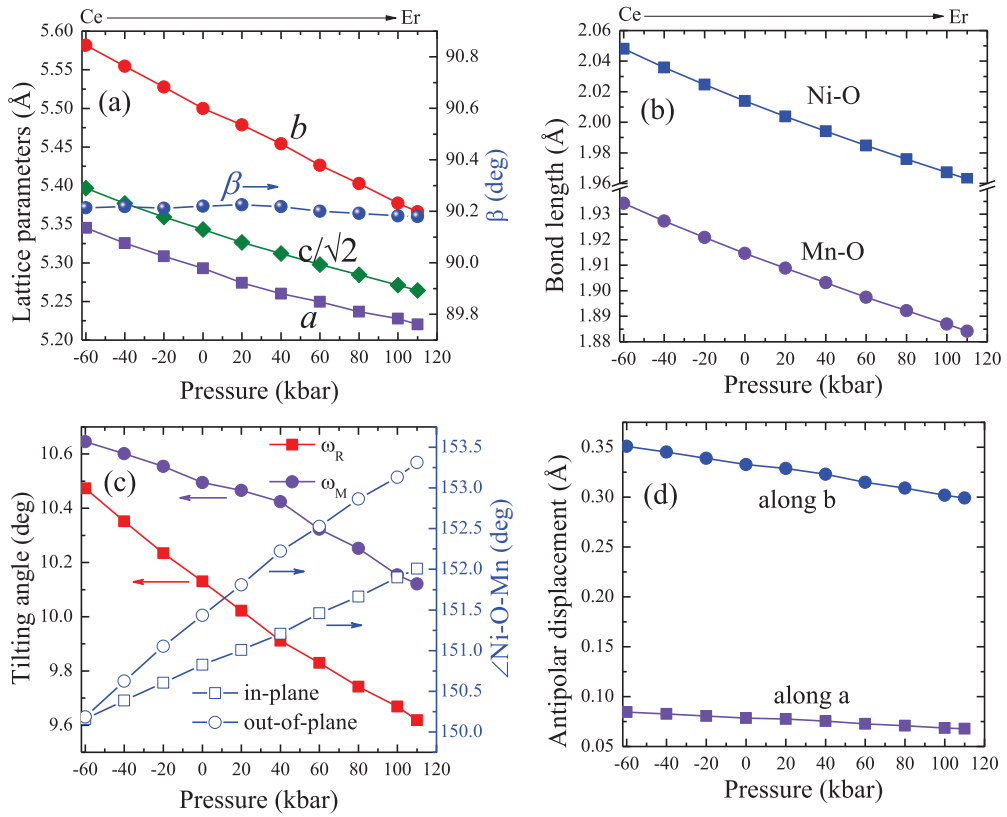

FIG. 3. (Color online) Similar to Fig. 1, but for Sm_2NiMnO_6 double perovskite as a function of hydrostatic pressure.

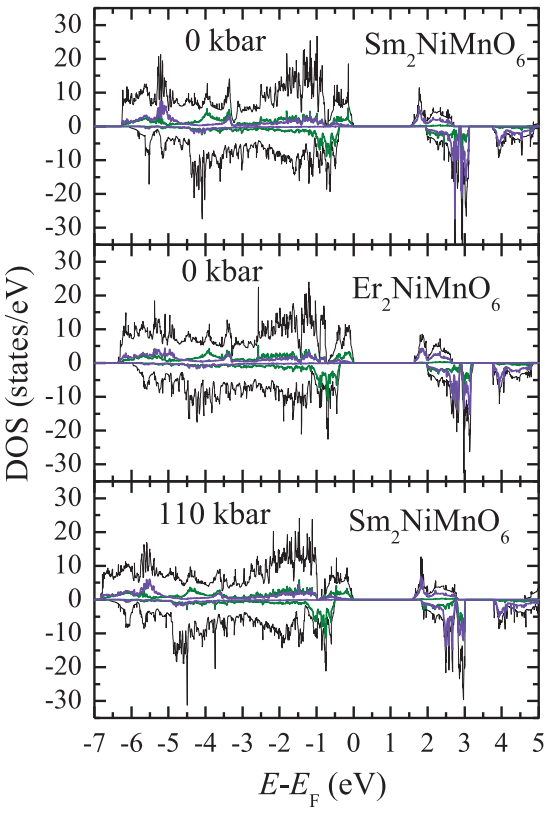

FIG. 5. (Color online) Calculated DOS of Sm_2NiMnO_6 (0 kbar, top panel), Er_2NiMnO_6 (0 kbar, middle panel), and Sm_2NiMnO_6 (110 kbar, bottom panel), respectively. The total DOS are shown by means of black lines, while the contribution of Ni 3*d* and Mn 3*d* bands are represented via green and purple lines, respectively. For each panel, the upper part shows the spin-up channel, and the bottom part depicts the results for the spin-down channel.

versus 150.2° to 153.3° for the out-of-plane angle) when the hydrostatic pressure increases from −60 to 110 kbar. Note also that the change in magnitude of ω_R and ω_M is much smaller when applying a hydrostatic pressure from −60 to 110 kbar in Sm_2NiMnO_6 (i.e., 0.9° and 0.5°, respectively) than when changing the rare-earth ion from R = Ce to Er in R_2NiMnO_6 (i.e., 4.2° and 7.6°, respectively). A much weaker response to the hydrostatic pressure and an opposite behavior between the application of hydrostatic and chemical pressures are also seen for the antipolar displacements along the *a* and *b* directions [cf. Figs. 1(d) and 3(d)] as well as for the magnetic Curie temperature (cf. Figs. 2 and 4). It is also interesting to realize that the inset of Fig. 4 shows that a perfect linear relationship between T_C and $\langle\cos^2\theta\rangle$ remains valid for Sm_2NiMnO_6 under hydrostatic pressure, therefore further emphasizing the importance of the Ni-O-Mn exchange angles in the control of the Curie temperature of R_2NiMnO_6 systems.

Figure 5 shows the calculated densities of state (DOS) of Sm_2NiMnO_6 (at 0 kbar), Er_2NiMnO_6 (at 0 kbar), and Sm_2NiMnO_6 (at 110 kbar), respectively. In all cases, the main contribution from the band extending from −7 eV to the Fermi level, E_F (chosen as the zero in energy) is found to be (not shown here) from the O 2*p* states, both for the spin-up and spin-down channels. Moreover, Ni 3*d* and Mn 3*d* states also contribute to the spin-up channel of that valence band, with these 3*d* states spreading over the whole energy range from ca. −7 eV to E_F of that spin-up channel and with Ni 3*d* states being more predominant than Mn 3*d* states near E_F in that spin-up channel. Moreover, Ni 3*d*, but not Mn 3*d*, states heavily participate in the spin-down channel of the valence band, especially in the vicinity of the Fermi level. In contrast, the main contribution to the bottom of the conduction band (spin-up channel) among the B atoms is from the Mn 3*d* states for the three cases shown in Fig. 5. Therefore, the band gap of R_2NiMnO_6 under both chemical pressure and hydrostatic pressure opens (by crystal field splitting) from the spin-up channel of Ni 3*d* states (Ni e_g states) of the valence band to the spin-up channel of Mn 3*d* states (Mn e_g states) of the conduction band, in agreement with a previous calculation [25]. Interestingly, the DOS of Sm_2NiMnO_6 and Er_2NiMnO_6 at 0 kbar are very similar, in the sense that they mostly "only" differ by the energetic position of the conduction band minimum with respect to the Fermi level. This fact reveals that the chemical pressure mainly "only" affects the value of the electronic band gap of R_2NiMnO_6 oxides. On the other

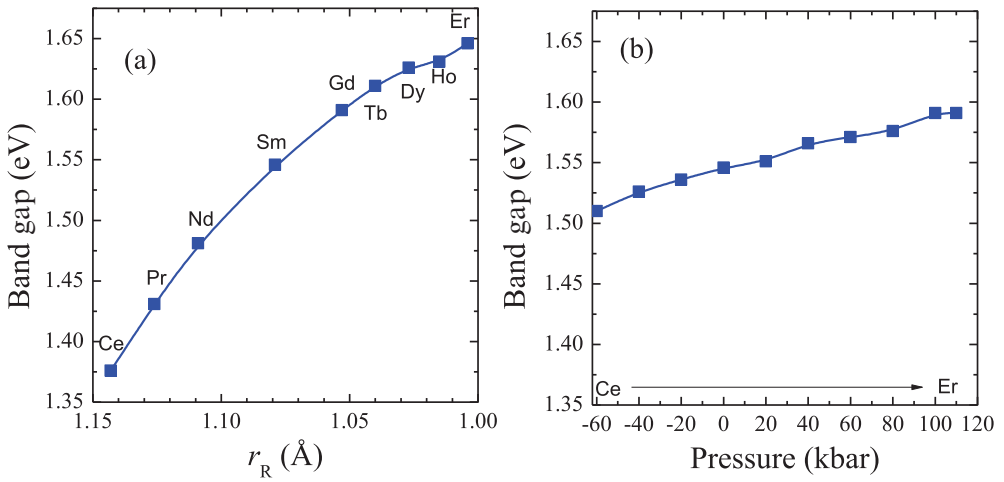

FIG. 6. (Color online) Band gap of (a) R_2NiMnO_6 as a function of chemical pressure and of (b) Sm_2NiMnO_6 as a function of hydrostatic pressure.

hand, when comparing the DOS plots of Sm_2NiMnO_6 at 0 kbar versus 110 kbar, one can see that (i) the valence band expands and shifts to lower energy under hydrostatic pressure and (ii) the spin-up and spin-down channels of the conduction band for the 110-kbar case become closer to each other in energy.

Finally, Fig. 6 displays the electronic band gap of R_2NiMnO_6 under chemical pressure and that of Sm_2NiMnO_6 under hydrostatic pressure. Three characteristics are shown here: (i) the band gaps of R_2NiMnO_6 increase as r_R decreases, which is consistent with the experimental results shown in Ref. [1] (note, however, that our numerical scheme tends to overestimate the band gap with respect to the data of Ref. [1]; for instance, we predict a value of about 1.55 eV for Sm_2NiMnO_6, compared with the measurement of 1.23 eV for that compound in Ref. [1]); (ii) the band gap of Sm_2NiMnO_6 also increases as the hydrostatic pressures increases; and (iii) the changing value of the electronic band gap of R_2NiMnO_6 with chemical pressure (from ∼1.37 to 1.65 eV) is 3.5 times of that for Sm_2NiMnO_6 with hydrostatic pressure (from ∼1.51 to 1.59 eV).

We also perform calculations on Dy_2NiMnO_6 (i.e., replace Sm by Dy) under hydrostatic pressure to confirm the generality of our conclusions. We also found (not shown here) that results in that compound are similar to those mentioned for Sm_2NiMnO_6 under hydrostatic pressure. Examples include: (i) all the lattice parameters and the averaged Ni-O and Mn-O bond lengths almost linearly decrease with increasing hydrostatic pressure, with the relationship $b > c/\sqrt{2} > a$ being valid for any hydrostatic pressure; (ii) the monoclinic angle, the oxygen octahedral tilting angles, and antipolar displacements do not significantly change with hydrostatic pressure; and (iii) the electronic band gap and magnetic transition temperature only slightly increase with hydrostatic pressure, with T_C still being nearly linear dependent on $\langle\cos^2\theta\rangle$.

IV. CONCLUSION

In summary, the effects of chemical and hydrostatic pressures on structural, magnetic, and electronic properties of double perovskite R_2NiMnO_6 oxides have been systematically investigated by first-principles calculations. The experimentally observed dependence of the lattice parameters, monoclinic angle, Ni-O-Mn bond angles, magnetic Curie temperature, and electronic band gap with the rare-earth ionic radius, as well as the remarkable linear relationship between the magnetic Curie temperature and the mean average of the square of the cosine of the Ni-O-Mn bond angles, are all well reproduced by the simulations. Moreover, these simulations also offer novel predictions that call for experimental confirmation, including (i) the dramatic quantitative and even qualitative difference in response of structural, magnetic, and electronic properties to hydrostatic *versus* chemical pressure and (ii) the dependency of antipolar displacements on these two different types of pressures. Furthermore, it is important to realize that the numerical data reported here and the insight they provide can also lead to the future development of atomistic schemes (such as effective Hamiltonians [21,26], shell models [27], bond-valence models [28], and tight-binding-like approaches [29]) or phenomenological Landau-type potentials [30], whose use would allow the predictions of *finite-temperature* properties of these important materials. For instance, the fact that the antipolar displacements shown in Fig. 1(d) increase when decreasing the size of the rare-earth element implies that, in a Landau-type expansion, the coefficient appearing in front of the square of the AFE vector will become more negative as the rare-earth ionic radius decreases. On the other hand, the fact that these antipolar displacements decrease when increasing the hydrostatic pressure [see Fig. 3(d)] can be understood by realizing that hydrostatic pressure leads to a decrease of the strain and that such decrease results in a reduction of the antipolar displacements because of the well-known coupling between strain and cationic displacements. Such double interaction (between pressure and strain, and between strain and cationic displacement) would have to be included in the aforementioned atomic schemes and phenomenologies for them to be realistic. We thus hope that the present paper will be of benefits to the scientific community.

ACKNOWLEDGMENTS

The present paper is supported by the National Natural Science Foundation of China under Grants No. 51332006 (X.M.C. and H.J.Z.) and 11274270 (X.M.C.) and by the ARO Grant W911NF-12-1-0085 (L.B.). Some computations were also made possible thanks to NSF MRI Grant No. 0722625, NSF MRI-R2 Grant No. 0959124, NSF Grant No. 0918970, and a Challenge grant from the U.S. Department of Defense.

[1] C. L. Bull and P. F. McMillan, J. Solid State Chem. **177**, 2323 (2004).
[2] R. J. Booth, R. Fillman, H. Whitaker, A. Nag, R. M. Tiwari, K. V. Ramanujachary, J. Gopalakrishnan, and S. E. Lofland, Mater. Res. Bull. **44**, 1559 (2009).
[3] W. Z. Yang, X. Q. Liu, H. J. Zhao, Y. Q. Lin, and X. M. Chen, J. Appl. Phys. **112**, 064104 (2012).
[4] D. C. Kakarla, K. M. Jyothinagaram, A. K. Das, and V. Adyam, J. Am. Ceram. Soc. **97**, 2858 (2014).
[5] N. S. Rogado, J. Li, A. W. Sleight, and M. A. Subramanian, Adv. Mater. **17**, 2225 (2005).
[6] D. Choudhury, P. Mandal, R. Mathieu, A. Hazarika, S. Rajan, A. Sundaresan, U. V. Waghmare, R. Knut, O. Karis, P. Nordblad, and D. D. Sarma, Phys. Rev. Lett. **108**, 127201 (2012).
[7] M. P. Singh, K. D. Truong, S. Jandl, and P. Fournier, Phys. Rev. B **79**, 224421 (2009).
[8] H. Guo, A. Gupta, M. Varela, S. Pennycook, and J. Zhang, Phys. Rev. B **79**, 172402 (2009).
[9] R. Shannon, Acta Crystallogr. Sect. A **32**, 751 (1976).
[10] H. J. Zhao, J. Íñiguez, W. Ren, X. M. Chen, and L. Bellaiche, Phys. Rev. B **89**, 174101 (2014).
[11] J. M. Rondinelli and C. J. Fennie, Adv. Mater. **24**, 1961 (2012).

[12] A. T. Mulder, N. A. Benedek, J. M. Rondinelli, and C. J. Fennie, Adv. Funct. Mater. **23**, 4810 (2013).
[13] H. J. Zhao, W. Ren, Y. Yang, J. Íñiguez, X. M. Chen, and L. Bellaiche, Nat. Commun. **5**, 4021, (2014) .
[14] D. Kan, L. Pálová, V. Anbusathaiah, C. J. Cheng, S. Fujino, V. Nagarajan, K. M. Rabe, and I. Takeuchi, Adv. Funct. Mater. **20**, 1108 (2010).
[15] G. Kresse and D. Joubert, Phys. Rev. B **59**, 1758 (1999).
[16] J. P. Perdew, A. Ruzsinszky, G. I. Csonka, O. A. Vydrov, G. E. Scuseria, L. A. Constantin, X. Zhou, and K. Burke, Phys. Rev. Lett. **100**, 136406 (2008).
[17] H. J. Zhao, W. Ren, Y. Yang, X. M. Chen, and L. Bellaiche, J. Phys.: Condens. Matter **25**, 466002 (2013).
[18] H. J. Zhao, W. Ren, X. M. Chen, and L. Bellaiche, J. Phys.: Condens. Matter **25**, 385604 (2013).
[19] J. P. Perdew, K. Burke, and M. Ernzerhof, Phys. Rev. Lett. **77**, 3865 (1996).
[20] A. Glazer, Acta Crystallogr. Sect. B **28**, 3384 (1972).
[21] I. A. Kornev, L. Bellaiche, P.-E. Janolin, B. Dkhil, and E. Suard, Phys. Rev. Lett. **97**, 157601 (2006).
[22] S. Prosandeev, D. Wang, W. Ren, J. Íñiguez, and L. Bellaiche, Adv. Funct. Mater. **23**, 234 (2013).
[23] L. Bellaiche and J. Íñiguez, Phys. Rev. B **88**, 014104 (2013).
[24] J.-S. Zhou, J. A. Alonso, V. Pomjakushin, J. B. Goodenough, Y. Ren, J.-Q. Yan, and J.-G. Cheng, Phys. Rev. B **81**, 214115 (2010).
[25] H. J. Zhao and X. M. Chen, AIP Adv. **2**, 042143 (2012).
[26] W. Zhong, D. Vanderbilt, and K. M. Rabe, Phys. Rev. Lett. **73**, 1861 (1994).
[27] M. Sepliarsky, S. R. Phillpot, D. Wolf, M. G. Stachiotti, and R. L. Migoni, Appl. Phys. Lett. **76**, 3986 (2000).
[28] Y.-H. Shin, V. R. Cooper, I. Grinberg, and A. M. Rappe, Phys. Rev. B **71**, 054104 (2005).
[29] A. Chattopadhyay and A. J. Millis, Phys. Rev. B **64**, 024424 (2001).
[30] M. Mostovoy, Phys. Rev. Lett. **96**, 067601 (2006).